The Astrophysical Journal Letters, 1002:L29 (7pp), 2026 May 1 https://doi.org/10.3847/2041-8213/ae6270

Blue Straggler in the Making: An X-Ray Active Binary in Algol Configuration

A. H. Sheikh[1], Biman J. Medhi[1], Annapurni Subramaniam[2], Sergio Messina[3], Susmita Das[4], Hitendra Sarkar[1], Anupam Bhardwaj[4], Atila Poro[5], Marina Kounkel[6], and Ram Sagar[2]
[1] Department of Physics, Gauhati University, Guwahati 781014, Assam, India; asheikh@gauhati.ac.in
[2] Indian Institute of Astrophysics, Block II, Koramangala, Bangalore 560034, India
[3] INAF—Catania Astrophysical Observatory, via S. Sofia 78, 95123 Catania, Italy
[4] Inter University Centre for Astronomy & Astrophysics, Pune 411007, India
[5] LUX, Observatoire de Paris, CNRS, PSL, 61 Avenue de l'Observatoire, 75014 Paris, France
[6] Department of Physics and Astronomy, University of North Florida, Jacksonville, FL 32224, USA
Received 2026 April 10; revised 2026 April 20; accepted 2026 April 21; published 2026 April 30

Abstract

We report an extremely rare X-ray active blue straggler star (BSS) in Collinder 261, undergoing ongoing Roche-lobe overflow in a semidetached binary in an Algol-type configuration with an orbital period of $P_{\rm orb} \sim 2.112$ days, providing direct observational evidence for the ongoing binary mass-transfer formation channel of BSS. Light-curve modeling with PHOEBE reveals a low mass ratio of $q \sim 0.19$, corresponding to a mass of 1.67 $M_{\odot}$for the BSS primary and a mass of 0.32 $M_{\odot}$ for the Roche-lobe-filling companion. Reflection effects and a hotspot near the inner Lagrangian point (L_1) reproduce the observed light-curve asymmetries, while the observed X-ray luminosity is consistent with direct-impact accretion-driven emission, supporting ongoing mass transfer. Radial velocities from the Very Large Telescope/GIRAFFE are also consistent with the photometric solution and reveal enhanced primary rotation of $v \sin i \sim 69.55$ km s^{-1}, consistent with spin-up through direct-impact accretion. Evolutionary modeling with MESA reproduces the observed configuration for an initially detached system with $M_d \sim 1.12\ M_{\odot}$, $M_a \sim 0.92\ M_{\odot}$, and $P_{\rm ini} \sim 0.83$ day. Roche-lobe overflow and mass transfer begin at ∼5.46 Gyr with mass ratio reversal at ∼5.58 Gyr. The present configuration at ∼7 Gyr, consistent with the cluster age, corresponds to stable mass transfer of $\dot{M} \sim 2 \times 10^{-10}\ M_{\odot}$ yr^{-1}. These results indicate that the system represents a very rare case of a BSS currently forming through binary mass transfer.

Unified Astronomy Thesaurus concepts: Stellar astronomy (1583); Close binary stars (254); Blue straggler stars (168); Algol variable stars (24); Stellar dynamics (1596)

1. Introduction

Blue straggler stars (BSSs) are anomalous stars in clusters that appear brighter and bluer than the main-sequence turnoff (MSTO; A. R. Sandage 1953). Since cluster stars are generally coeval, the presence of stars above the MSTO cannot be explained by standard single-star evolution, making BSSs a long-standing problem in stellar evolution, with their formation pathways still debated and lacking clarity (H. M. J. Boffin et al. 2015; A. M. Geller et al. 2015; A. H. Sheikh & B. J. Medhi 2024a; A. H. Sheikh et al. 2025). Several formation mechanisms have been proposed. One major pathway involves binary evolution, where mass transfer (MT) from an evolving companion rejuvenates the accreting star, sometimes followed by a merger (W. H. McCrea 1964). BSSs can also form through direct stellar collisions or dynamical interactions in dense cluster environments (J. G. Hills & C. A. Day 1976; A. Sills & C. D. Bailyn 1999; S. Chatterjee et al. 2013). Another channel involves hierarchical triple systems, where Kozai–Lidov cycles can drive mergers in the inner binary (H. B. Perets & D. C. Fabrycky 2009; S. Naoz & D. C. Fabrycky 2014; A. H. Sheikh et al. 2026). The dominant mechanism depends on the environment, with binary evolution particularly important in open clusters. MT can occur at different donor evolutionary stages. Case A MT, involving a main-sequence donor, typically produces very short-period binaries and can lead to common-envelope (CE) evolution or mergers, which are relatively rare among BSSs (X. Chen & Z. Han 2008). Case B MT, with a red giant donor, generally results in BSS binaries with periods of a few days and helium white dwarf companions (W. H. McCrea 1964; R. F. Webbink 1976; M. Sun et al. 2021). Case C MT, occurring during the asymptotic giant branch phase, produces long-period systems with carbon–oxygen white dwarf companions, both of which are commonly observed (R. Kippenhahn et al. 1967; X. Chen & Z. Han 2007). Observational surveys also indicate a Case A MT channel is relatively rare, as the binary period distribution of BSSs peaks at longer periods and frequently features white dwarf companions indicative of later-stage (Case B/C) MT (R. D. Mathieu & A. M. Geller 2009; N. M. Gosnell et al. 2014). Another possible channel is the merger of two MSTO stars during post-main-sequence evolution (V. V. Jadhav & A. Subramaniam 2021).

In our study, we explore and give support to the hypothesis that BSSs can form via stable Algol-type MT, which has also been well established by M. A. Giannuzzi (1984). In fact, M. A. Giannuzzi (1984) emphasized the importance of identifying such systems in open clusters to test this scenario observationally. In addition, several binary systems have already been identified that exhibit properties consistent with this evolutionary channel, including post-MT or semidetached configurations (K. Stępień et al. 2017). Binary systems with extreme mass ratios and short orbital periods provide important constraints on BSS MT histories (W. H. McCrea 1964). The presence of low-mass, inflated secondaries in semidetached configurations indicates ongoing, stable MT rather than merger-

dominated pathways. Although such systems are rarely observed during active mass exchange, they are consistent with Algol-type evolution and support stable MT as an important BSS formation channel (X. Chen & Z. Han 2008; E. Leiner et al. 2019).

In this work, we investigate Gaia DR3 5856515601255190272 (R.A. (α) = $12^h38^m16^s.558$, decl. (δ) = $-68°25'18''.946$), a BSS candidate in Collinder 261 that has counterparts in Chandra X-ray observations. Collinder 261 ($\alpha = 12^h37^m57^s$, $\delta = -68°22'00''$) is among the oldest known open clusters, with an estimated age of ~7 Gyr and located at a distance of ~2.9 kpc (S. Vats & M. van den Berg 2017; M. J. Rain et al. 2020; X. Gao 2023). This BSS is classified as an eclipsing binary with an orbital period of 2.11 days, having $G_{mag} = 14.244 \pm 0.001$ and $V_{mag} = 14.361 \pm 0.092$ (D. E. McLaughlin & R. P. van der Marel 2005; S. Vats & M. van den Berg 2017; M. J. Rain et al. 2020). S. Vats & M. van den Berg (2017) identified this system as an X-ray-active BSS (CX18/V45) in an eclipsing binary configuration, but its physical nature and evolutionary state remained unclear, particularly whether it is currently undergoing MT. Here, we refine its characterization using confirmed cluster membership, improved light curves (LCs), and MESA modeling. Combining photometric and spectroscopic constraints with theoretical modeling, we suggest that the system is a semidetached, Algol-type binary undergoing active MT with an extreme mass ratio, in which the secondary fills its Roche lobe. While Algol-type BSS systems have been reported in globular clusters (J. Kaluzny et al. 2007; G. Kumawat et al. 2024), to our knowledge, such systems have not been well established in open clusters. We therefore present the first detailed analysis of such a system in an open cluster and model its evolution to constrain its MT-driven formation pathway, providing strong observational support for this channel (M. A. Giannuzzi 1984). This provides an extremely rare and well-constrained example of an Algol-type MT mechanism leading to the formation of a BSS. The remaining Letter is organized as follows: In Section 2, we describe the datasets used in this work. The methodology is presented in Section 3, and the results and conclusions are discussed in Section 4.

2. Data Used

2.1. Radial Velocity Data

The target BSS was observed with the Fibre Large Array Multi Element Spectrograph (FLAMES) on the Very Large Telescope (VLT) at the European Southern Observatory (ESO), Paranal, Chile, under program ID 109.22ZM. The GIRAFFE spectrograph was used in medium-resolution mode with the HR12 setup, covering 581.4−614.4 nm at a resolving power of $R \sim 18{,}000$. The target was observed in six epochs, each with an exposure time of about 2730 s. The spectra are obtained from the ESO Science Archive Facility. Since the data are already Phase 3 reduced, only sky subtraction and continuum normalization were performed using the `specutils` Python package. Radial velocities (RVs) of the primary star are determined using an iterative cross-correlation method. Each normalized spectrum is cross correlated with the first spectrum as the initial template over a velocity range of ± 200 km s^{-1}, and RV shifts are obtained by fitting a Gaussian to the peak of the cross-correlation function (CCF). A refined template is then constructed by Doppler shifting the spectra to the rest frame of the primary and median stacking them. This procedure is repeated until the RV differences between successive iterations are below 0.01 m s^{-1}. Finally, the relative RVs are placed on an absolute scale by cross correlating the final template with a synthetic atomic line mask for an A0-type star. We estimated the atmospheric parameters of the BSS primary using `iSpec` (S. Blanco-Cuaresma et al. 2014) by fitting synthetic spectra to selected absorption lines using predefined line masks and a least-squares optimization, as shown in Figure 1. The synthetic spectra are generated using `ATLAS9.KuruczODFNEW` atmospheric models (F. Castelli & R. L. Kurucz 2003) and the `MOOG` radiative transfer code (C. Sneden 1973). The derived parameters are listed in Table 1.

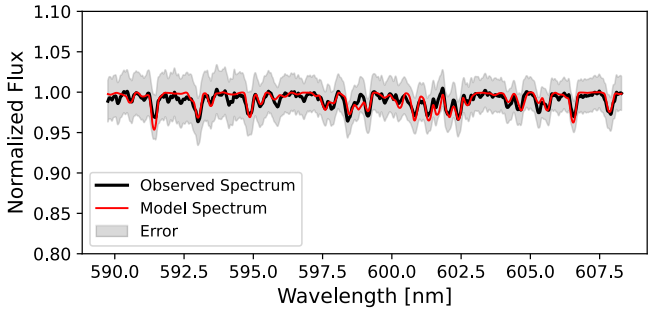

Figure 1. Synthetic spectral fitting of the BSS spectrum. The observed spectrum (black) is shown together with the best-fitting synthetic spectrum (red), with the gray shaded region indicating the uncertainties.

2.2. Light-curve Data

The target BSS (TIC 327546480) was observed in TESS Sector 11 through the TESS–Gaia Light Curve pipeline (TGLC; T. Han & T. D. Brandt 2023). The TGLC pipeline uses effective point-spread function modeling with Gaia DR3 priors to decontaminate target stars from nearby sources and minimize crowding effects. It achieves photometric precision of $\leqslant 2\%$ at 16th TESS magnitude, even in crowded fields. The LC for this BSS is extracted using the TGLC pipeline data release. We first performed a statistical cleaning of the LC and subsequently analyzed it using the `Lightkurve` Python package. Periodicities are identified using the Lomb–Scargle periodogram. To assess the signal significance, we computed the false alarm probability (FAP). The resulting FAP for the best peak is ($\ll 10^{-10}$), indicating a highly significant detection. The orbital period is found to be $P_{orb} = 2.112 \pm 0.003$ days and clearly displays the defining features of an eclipsing binary of the Algol-type (β-Persei) eclipsing binary, as illustrated in Figure 2(a). We compared the TESS LC with the photometric results of B. Mazur et al. (1995). The relative depths and overall morphology of the LC are in good agreement with those reported by B. Mazur et al. (1995).

3. Methodology

3.1. Binary Modeling

To model the observed RV variations caused by binary orbital motion, we adopt a standard Keplerian model. For a single-lined spectroscopic binary (SB1), the RVs of the primary as a function of time are given by

$$V(t) = \gamma + K[\cos(\theta(t) + \omega) + e\cos\omega], \quad (1)$$

where γ is the systemic velocity of the binary, K is the RV semiamplitude, ω is the argument of periastron, e is the orbital

Table 1
Derived Parameters of the System

Parameter	Value
Keplerian Orbit Model	
$P_{\rm orb}$ (days)	2.112 ± 0.001
V_γ (km s^{-1})	–29.22 ± 0.21
K (km s^{-1})	31.91 ± 0.35
e	0.03 ± 0.01
ω (deg)	71.51 ± 21.08
t_0 (BJD)	2458601.8925 ± 0.0003
Spectral Fit	
$T_{\rm BSS}$ (K)	7439 ± 132
$\log g_{\rm BSS}$	3.69 ± 0.37
(M/H)	–0.11 ± 0.02
$v \sin i$ (km s^{-1})	69.55 ± 3.76
PHOEBE Model	
q	0.19 ± 0.02
i (deg)	72.29 ± 0.39
a ($R_\odot$)	8.72 ± 0.42
$R_{\rm BSS}$ ($R_\odot$)	2.64 ± 0.13
$R_{\rm Donor}$ ($R_\odot$)	2.16 ± 0.10
$T_{\rm BSS}$ (K)	7439 ± 132
$T_{\rm Donor}$ (K)	4365 ± 128
b (deg)	90 (fixed)
l (deg)	6 ± 2
r (deg)	11 ± 3
$T_{\rm spot}$ (K)	8554 ± 558
$M_{\rm BSS}$ ($M_\odot$)	1.67 ± 0.24
$M_{\rm Donor}$ ($M_\odot$)	0.32 ± 0.08
$\log g_{\rm BSS}$	3.82 ± 0.07
$\log g_{\rm Donor}$	3.27 ± 0.08
$L_{\rm BSS}$ ($L_\odot$)	19.31 ± 2.51
$L_{\rm Donor}$ ($L_\odot$)	1.52 ± 0.28
MESA Model	
$P_{\rm orb}$ (days)	2.112
q	0.19
a ($R_\odot$)	8.71
$R_{\rm BSS}$ ($R_\odot$)	2.66
$R_{\rm Donor}$ ($R_\odot$)	2.17
$T_{\rm BSS}$ (K)	7367
$T_{\rm Donor}$ (K)	4552
$M_{\rm BSS}$ ($M_\odot$)	1.67
$M_{\rm Donor}$ ($M_\odot$)	0.32
$\log g_{\rm BSS}$	3.81
$\log g_{\rm Donor}$	3.27
$L_{\rm BSS}$ ($L_\odot$)	18.81
$L_{\rm Donor}$ ($L_\odot$)	1.82

eccentricity, and $\theta(t)$ is the angular position of the star from the center of mass at time t.

To estimate the orbital parameters and their uncertainties, we used Markov Chain Monte Carlo (MCMC) sampling using the `emcee` sampler (D. Foreman-Mackey et al. 2013). The resulting best-fit parameters are listed in Table 1. The RV measurements and model are phase folded, showing the periodic orbital motion, confirming the system as an SB 1. To derive the orbital and physical parameters of the system, we modeled the LC and RV curve using the PHysics Of Eclipsing BinariE code (`PHOEBE`; A. Prša et al. 2016; K. E. Conroy et al. 2020), assuming a semidetached configuration, since alternative configurations (detached or contact) do not provide satisfactory solutions to the observed LC and system geometry. The BSS temperature $T_{\rm BSS} = 7439 \pm 132$ K is adopted from the spectral fitting. The initial mass ratio ($q \sim 0.20$) is determined using a global q-search method. Given the temperature contrast between the components, we adopted bolometric albedos and gravity-darkening coefficients of $(g_1, A_1) = (1, 1)$ for the BSS and $(g_2, A_2) = (0.32, 0.6)$ for the donor. Stellar atmospheres are modeled using F. Castelli & R. L. Kurucz (2004) tables, and limb-darkening coefficients are treated as free parameters.

We fitted five parameters from initial guesses: semimajor axis (a), inclination (i), mass ratio (q), temperature of secondary ($T_{\rm Donor}$), and the radius of the BSS ($R_{\rm BSS}$) using tight Gaussian prior ranges to ensure convergence. The donor radius ($R_{\rm Donor}$) is fixed to its Roche-lobe value under the semidetached assumption. An initial parameter exploration and optimization are performed using the Nelder–Mead solver (J. A. Nelder & R. Mead 1965), followed by MCMC sampling with `emcee` (D. Foreman-Mackey et al. 2013) to obtain the final parameters, which are listed in Table 1. The LC shows an O'Connell effect, indicating asymmetry in the system that requires a hotspot, likely produced by the impact of the accretion stream from the donor onto the accretor near the inner Lagrangian point (L_1). The fitted spot parameters colatitude (b), longitude (l), spot radius (r), and spot temperature ($T_{\rm spot}$) are listed in Table 1, and the best-fit LC and RV models, along with the mesh plots showing the preferred spot location, are presented in Figure 2. The nonsinusoidal features near phase 0.00 arise from eclipse-related geometric and surface-brightness effects, including a Rossiter–McLaughlin distortion and the influence of a localized hotspot.

As a consistency check, we computed the ballistic trajectory of a gas stream launched from the L_1 point in the Roche potential as shown in Figure 3. For plausible initial conditions, the stream impacts the accretor at a longitude of $\sim 10^\circ$, in good agreement with the hotspot location inferred from the `PHOEBE` modeling. Small offsets are expected, since the ballistic calculation identifies the initial impact location, whereas the observed hotspot traces the region of maximum emission after the shocked gas spreads over the stellar surface.

3.2. Possible Evolutionary Status

To investigate the past and future evolution of this system, we used the binary module of the Modules for Experiments in Stellar Astrophysics (`MESA`; B. Paxton et al. 2011, 2015, 2018, 2019; A. S. Jermyn et al. 2023). The simulations assume a metallicity of $Z = 0.01$ from the spectral fitting. Given that the MSTO mass of Collinder 261 is $\sim 1.1\ M_\odot$ (A. Bragaglia & M. Tosi 2006), we adopted a slightly higher initial donor mass of $M_{\rm d} \sim 1.12\ M_\odot$ to ensure that the donor evolves off the MS within the cluster age. The initial parameters are selected through exploration of the parameter space to reproduce the observed system at ~ 7 Gyr while maintaining stable Roche-lobe overflow. In particular, the initial orbital period ($P_{\rm ini} \sim 0.83$ day) is constrained such that MT begins at the appropriate evolutionary stage. Similarly, the adopted accretor mass ($M_{\rm a} \sim 0.92\ M_\odot$) allows sufficient mass growth to match the observed BSS mass. We assume nearly conservative MT (efficiency $\sim 94\%$), ensuring stable, nuclear-timescale MT.[7]

[7] The `MESA` inlist used in this work is available on Zenodo: DOI: 10.5281/zenodo.19644925.

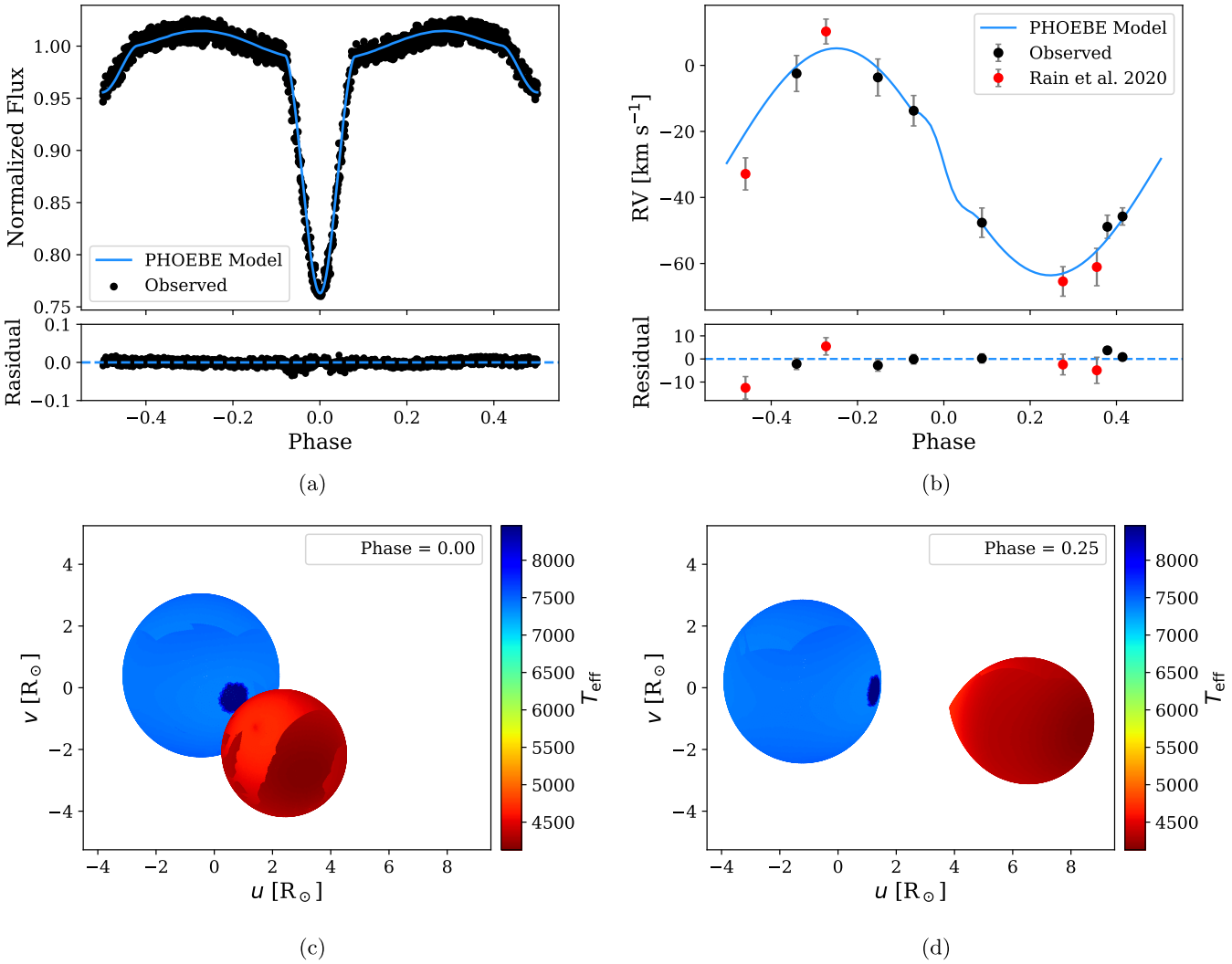

Figure 2. (a) The fitted LC with the PHOEBE model, with points representing the phase-folded data. (b) The fitted RV curve of the primary component with the PHOEBE model. (c) A mesh representation of the temperature distribution across the stellar photospheres, including a spot at phase 0.00, where the blue star is the BSS with a hotspot and the red star is the donor, respectively. (d) A mesh representation of the temperature distribution across the stellar photospheres, including a spot at phase 0.25, where the blue star is the BSS with a hotspot and the red star is the donor, respectively.

MT begins at 5.46 Gyr after the donor nearly exhausts its central hydrogen. To accurately model the Case B MT phase, we adopted weakened magnetic braking driven by global dynamo collapse in evolved stars (J. L. van Saders et al. 2016). During the evolution, the orbital period initially decreases to $P_{\rm orb} = 0.75$ day, and after the mass-ratio reversal at 5.58 Gyr, the orbit starts expanding. The system reaches its current configuration at an age of ∼7 Gyr, with a donor mass-loss rate of $\dot{M} \sim 2 \times 10^{-10}\, M_\odot\, {\rm yr}^{-1}$. At an age of 7.14 Gyr, the donor will evolve into a protohelium white dwarf of mass ∼0.29 $M_\odot$, while the accretor will become a subgiant filling its Roche lobe, marking the end of the stable MT phase. The MESA model yields system parameters that are consistent with the observed masses, orbital period, and the effective temperatures and radii of both the donor and accretor within the uncertainties of the PHOEBE-derived observational constraints, as shown in Figure 4.

The total accretion luminosity can be expressed as $L_{\rm acc} = \frac{GM_{\rm BSS}\dot{M}}{R_{\rm BSS}} = 1.51 \times 10^{31}\,{\rm erg\,s^{-1}}$. The Roche-lobe-filling secondary is a late-type K star possessing a convective envelope capable of sustaining magnetic dynamo activity. Such stars are known to produce strong coronal X-ray emission, reaching the saturated regime with $L_{\rm X}^{\rm coronal}/L \sim 10^{-3}$. This implies a maximum coronal X-ray luminosity of $L_{\rm X}^{\rm coronal} \sim 0.58 \times 10^{31}\,{\rm erg\,s^{-1}}$. The system is detected in Chandra X-ray

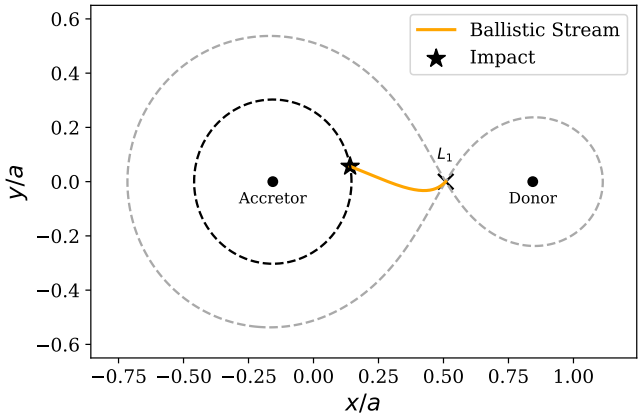

Figure 3. Ballistic stream trajectory in the Roche potential of the binary system.

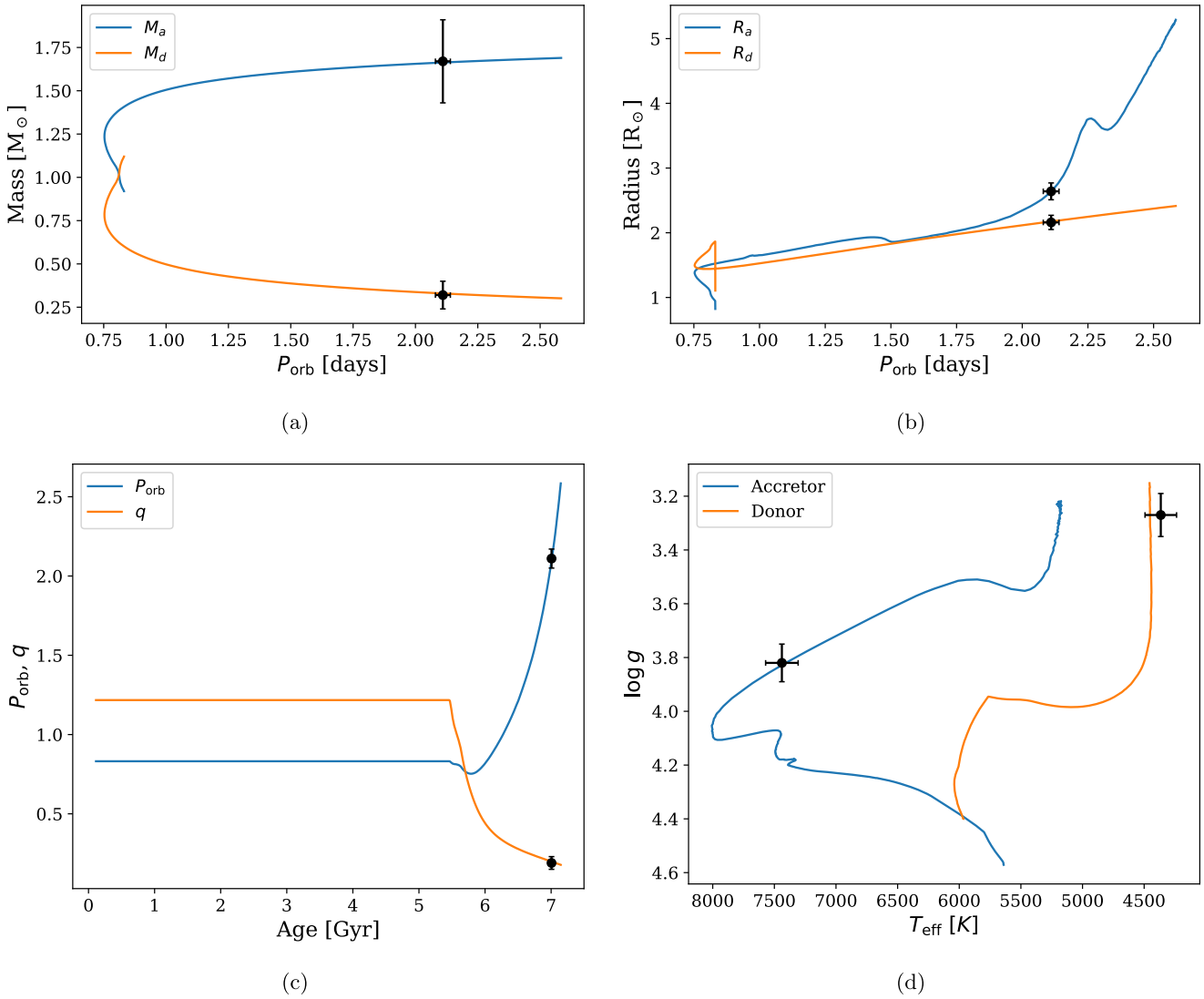

Figure 4. (a) Evolution of the donor (orange line) and accretor (blue line) masses as a function of orbital period, P_{orb}, during binary evolution. The filled point marks the present-day observed configuration. (b) Evolution of the donor (orange line) and accretor (blue line) radii as a function of P_{orb}. (c) Evolution of the orbital period, P_{orb} (blue line) and mass ratio, q (orange line) of the system. (d) Evolutionary tracks of the donor (orange line) and accretor (blue line) from the best-fit MESA model in the $\log g$–T_{eff} plane.

observation with a flux of $F_X \sim 2.07 \times 10^{-14}$ erg cm^2 s^{-1}, corresponding to a luminosity of $L_X \sim 2.1 \times 10^{31}$ erg s^{-1} (S. Wang et al. 2016). The observed X-ray luminosity can be interpreted as the sum of contributions from accretion-powered emission predicted by our binary evolution modeling and coronal activity in the donor star. The accretion luminosity arises when the donor star fills its Roche lobe and transfers material through the L_1, forming a gas stream that directly impacts the surface of the BSS accretor, while the donor contributes coronal emission due to magnetic activity driven by rapid rotation. The combined contribution, $L_X^{obs} \approx L_{accretion} + L_{coronal}$, naturally explains the observed X-ray luminosity, with accretion dominating and coronal emission providing a secondary component. We examined the available Chandra observation to search for orbital modulation of the X-ray emission, as expected if it originates from a localized accretion hotspot. In this scenario, the emission would be strongly phase dependent and could be suppressed when the hotspot is oriented away from the observer. However, the source is very faint, yielding only a few photons, and the observation covers only a fraction of the orbital period. No statistically significant phase-dependent modulation is detected. Deeper or dedicated X-ray observations are required to check for orbital modulation.

Binary evolution models computed with MESA reproduce the evolutionary state of the system, showing that Roche-lobe overflow began at ∼5.46 Gyr, followed by mass-ratio reversal at ∼5.58 Gyr, which led to the formation of a rejuvenated BSS through sustained accretion. At the present cluster age, the model predicts ongoing nearly conservative MT at a rate of $\dot{M} \sim 2 \times 10^{-10}\ M_\odot\,\mathrm{yr}^{-1}$. This mass-transfer rate yields an accretion luminosity that is consistent with the observed X-ray luminosity, supporting an accretion-powered origin for the dominant X-ray emission.

4. Results, Discussion, and Conclusion

The results obtained from this analysis are summarized as follows:

The combined LC and RV modeling using PHOEBE yields an orbital period of $P_{orb} = 2.112$ days and a low mass ratio of $q = 0.19$, indicating a strongly unequal-mass binary

corresponding to a mass of 1.67 $M_\odot$ for BSS primary and a mass of 0.32 $M_\odot$ for Roche-lobe-filling companion. The observed projected rotational velocity ($v \sin i = 69.55$ km s^{-1}) corresponds to $v \sim 73$ km s^{-1} for $i \sim 72.^\circ 29$. The expected rotational velocity of the BSS is $v_{\rm rot} \approx 65$ km s^{-1}. This suggests that the BSS primary is rotating near the synchronous velocity, consistent with spin-up due to ongoing mass accretion. We estimated a characteristic spin-up timescale of $t_{\rm spin} \sim 0.1$ Gyr, which is significantly shorter than the MT timescale of ∼1.6 Gyr. Since $t_{\rm spin} \ll t_{\rm MT}$, the accretor can be efficiently spun up during the MT phase, supporting the interpretation that its near-synchronous rotation is a consequence of ongoing accretion.

Binary evolution models computed with MESA reproduce the observed configuration, starting from an initially detached system with a 1.12 $M_\odot$ donor and a 0.92 $M_\odot$ accretor with a period of 0.83 days. Roche-lobe overflow begins at ∼5.46 Gyr following central hydrogen exhaustion, leading to mass-ratio reversal and orbital expansion. At the current cluster age, the system undergoes stable MT at a rate of $\dot{M} \sim 2 \times 10^{-10}$ $M_\odot$ yr^{-1}, and is expected to evolve into a BSS with a ∼0.29 $M_\odot$ protohelium white dwarf companion. The observed X-ray emission is naturally explained by ongoing MT. Material transferred through the L_1 point directly impacts the BSS surface, producing shocks that heat the plasma to X-ray-emitting temperatures, while the donor may contribute a secondary component through coronal X-ray emission. Together with the hotspot inferred from LC modeling, these results provide strong evidence for ongoing Roche-lobe overflow. The system has been undergoing MT for ∼1.6 Gyr, during which the accretor has gained ∼0.75 $M_\odot$, consistent with its present mass. The assumed nearly conservative MT and weak magnetic braking imply stable, nuclear-timescale evolution, supporting a robust binary mass-transfer formation pathway for the BSS.

Looking ahead, the system is expected to continue stable MT until the donor loses most of its hydrogen-rich envelope and detaches, leaving behind a low-mass helium white dwarf. The accretor will remain as a rejuvenated BSS and later evolve off the main sequence. The system will then appear as a short-period BSS-helium white dwarf binary, similar to those observed in open clusters (A. Panthi et al. 2024; A. H. Sheikh & B. J. Medhi 2024a, 2024b). As the BSS evolves toward the red giant phase, it is expected to fill its Roche lobe, initiating a second phase of MT. Given the extreme mass ratio at this stage, the MT is likely to be dynamically unstable, leading to a CE phase. During this phase, the system may undergo orbital shrinkage. If the envelope is successfully ejected without a merger, the system may emerge as a close binary consisting of the stripped core of the BSS, which may appear as a subdwarf star or a helium white dwarf, and the preexisting helium white dwarf companion, as reported in the literatures (C. Koen et al. 1998; W. R. Brown et al. 2020; X.-C. Meng & Y.-P. Luo 2021; Y. Zhang et al. 2024). Alternatively, if the envelope ejection is inefficient, the system may merge to form a single overmassive giant, as suggested by K. Brogaard et al. (2018). The combined evidence of a Roche-lobe-filling donor, direct-impact accretion geometry, hotspot-induced LC asymmetry, and X-ray emission consistent with accretion shocks demonstrates that this system is a BSS currently forming through binary MT, providing an extremely rare observational insight into this process in action.

Acknowledgments

We thank the anonymous referee for the valuable comments and suggestions that helped us to improve the quality of our Letter. A.H.S. highly acknowledges the Department of Science and Technology (DST), Govt. of India, for providing the DST INSPIRE fellowship vide grant No. IF230175. A.B. acknowledges the funding from the Anusandhan National Research Foundation (ANRF) under the Prime Minister Early Career Research grant scheme (ANRF/ECRG/2024/000675/PMS). We thank Dr. Meng Sun (CIERA, Northwestern University) for insightful discussions on the MESA modeling. This work is based on data obtained from the ESO Science Archive Facility (European Southern Observatory ESO 2015). We made use of NASA's Astrophysics Data System as well as the VizieR and Simbad databases at CDS, Strasbourg, France. We acknowledge the Inter-University Centre for Astronomy and Astrophysics (IUCAA), Pune, for providing access to the Pegasus High Performance Computing facility.

ORCID iDs

A. H. Sheikh https://orcid.org/0009-0009-0399-0381
Biman J. Medhi https://orcid.org/0000-0002-3448-8150
Annapurni Subramaniam https://orcid.org/0000-0003-4612-620X
Sergio Messina https://orcid.org/0000-0002-2851-2468
Susmita Das https://orcid.org/0000-0003-3679-2428
Hitendra Sarkar https://orcid.org/0009-0004-5036-3202
Anupam Bhardwaj https://orcid.org/0000-0001-6147-3360
Atila Poro https://orcid.org/0000-0002-0196-9732
Marina Kounkel https://orcid.org/0000-0002-5365-1267
Ram Sagar https://orcid.org/0000-0003-4973-4745

References

Blanco-Cuaresma, S., Soubiran, C., Heiter, U., & Jofré, P. 2014, A&A, 569, A111
Boffin, H. M. J., Carraro, G., Beccari, G., et al. 2015, Ecology of Blue Straggler Stars (Springer), 413
Bragaglia, A., & Tosi, M. 2006, AJ, 131, 1544
Brogaard, K., Christiansen, S. M., Grundahl, F., et al. 2018, MNRAS, 481, 5062
Brown, W. R., Kilic, M., Bédard, A., Kosakowski, A., & Bergeron, P. 2020, ApJL, 892, L35
Castelli, F., & Kurucz, R. L. 2003, IAUS, 210, A20
Castelli, F., & Kurucz, R. L. 2004, A&A, 419, 725
Chatterjee, S., Rasio, F. A., Sills, A., & Glebbeek, E. 2013, ApJ, 777, 106
Chen, X., & Han, Z. 2007, AIPC, 948, 431
Chen, X., & Han, Z. 2008, MNRAS, 384, 1263
Conroy, K. E., Kochoska, A., Hey, D., et al. 2020, ApJS, 250, 34
European Southern Observatory (ESO) 2015, GIRAFFE/MEDUSA Reduced Data Obtained by Standard ESO Pipeline Processing, European Southern Observatory (ESO)
Foreman-Mackey, D., Hogg, D. W., Lang, D., & Goodman, J. 2013, PASP, 125, 306
Gao, X. 2023, PASJ, 75, 82
Geller, A. M., Latham, D. W., & Mathieu, R. D. 2015, AJ, 150, 97
Giannuzzi, M. A. 1984, A&A, 140, 373
Gosnell, N. M., Mathieu, R. D., Geller, A. M., et al. 2014, ApJL, 783, L8
Han, T., & Brandt, T. D. 2023, AJ, 165, 71
Hills, J. G., & Day, C. A. 1976, ApJL, 17, 87
Jadhav, V. V., & Subramaniam, A. 2021, MNRAS, 507, 1699
Jermyn, A. S., Bauer, E. B., Schwab, J., et al. 2023, ApJS, 265, 15
Kaluzny, J., Thompson, I. B., Rucinski, S. M., et al. 2007, AJ, 134, 541
Kippenhahn, R., Weigert, A., & Hofmeister, E. 1967, MComP, 7, 129
Koen, C., Orosz, J. A., & Wade, R. A. 1998, MNRAS, 300, 695
Kumawat, G., Heinke, C. O., Cohn, H. N., & Lugger, P. M. 2024, MNRAS, 530, 82

Leiner, E., Mathieu, R. D., Vanderburg, A., Gosnell, N. M., & Smith, J. C. 2019, ApJ, 881, 47
Mathieu, R. D., & Geller, A. M. 2009, Natur, 462, 1032
Mazur, B., Krzeminski, W., & Kaluzny, J. 1995, MNRAS, 273, 59
McCrea, W. H. 1964, MNRAS, 128, 147
McLaughlin, D. E., & van der Marel, R. P. 2005, ApJS, 161, 304
Meng, X.-C., & Luo, Y.-P. 2021, MNRAS, 507, 4603
Naoz, S., & Fabrycky, D. C. 2014, ApJ, 793, 137
Nelder, J. A., & Mead, R. 1965, CompJ, 7, 308
Panthi, A., Vaidya, K., Vernekar, N., et al. 2024, MNRAS, 527, 8325
Paxton, B., Bildsten, L., Dotter, A., et al. 2011, ApJS, 192, 3
Paxton, B., Marchant, P., Schwab, J., et al. 2015, ApJS, 220, 15
Paxton, B., Schwab, J., Bauer, E. B., et al. 2018, ApJS, 234, 34
Paxton, B., Smolec, R., Schwab, J., et al. 2019, ApJS, 243, 10
Perets, H. B., & Fabrycky, D. C. 2009, ApJ, 697, 1048
Prša, A., Conroy, K. E., Horvat, M., et al. 2016, ApJS, 227, 29
Rain, M. J., Carraro, G., Ahumada, J. A., et al. 2020, AJ, 159, 59
Sandage, A. R. 1953, AJ, 58, 61
Sheikh, A. H., & Medhi, B. J. 2024a, AJ, 168, 274
Sheikh, A. H., & Medhi, B. J. 2024b, MNRAS, 534, 4031
Sheikh, A. H., Medhi, B. J., Messina, S., et al. 2026, MNRAS, 545, staf2130
Sheikh, A. H., Medhi, B. J., & Sagar, R. 2025, ApJ, 989, 16
Sills, A., & Bailyn, C. D. 1999, ApJ, 513, 428
Sneden, C. 1973, ApJ, 184, 839
Stępień, K., Pamyatnykh, A. A., & Rozyczka, M. 2017, A&A, 597, A87
Sun, M., Mathieu, R. D., Leiner, E. M., & Townsend, R. H. D. 2021, ApJ, 908, 7
van Saders, J. L., Ceillier, T., Metcalfe, T. S., et al. 2016, Natur, 529, 181
Vats, S., & van den Berg, M. 2017, ApJ, 837, 130
Wang, S., Liu, J., Qiu, Y., et al. 2016, ApJS, 224, 40
Webbink, R. F. 1976, ApJ, 209, 829
Zhang, Y., Li, Z., Chen, X., & Han, Z. 2024, ApJ, 977, 24